

Ultra-Flat Galaxies Selected from RFGC Catalog. III. Star Formation Rate

O. V. Melnyk,^{1,*} V. E. Karachentseva,² and I. D. Karachentsev^{3,**}

¹*University of Zagreb, Zagreb, 10000 Croatia*

²*Main Astronomical Observatory of National Academy of Sciences of Ukraine, Kiev, 03143 Ukraine*

³*Special Astrophysical Observatory of the Russian AS, Nizhnij Arkhyz 369167, Russia*

(Received December 21, 2016; Revised January 03, 2017)

We examine the star formation properties of galaxies with very thin disks selected from the Revised Flat Galaxy Catalog (RFGC). The sample contains 333 ultra-flat galaxies (UFG) at high Galactic latitudes, $|b| > 10^\circ$, with a blue major angular diameter of $a \geq 1'.2$, blue and red apparent axial ratios of $(a/b)_b > 10$, $(a/b)_r > 8.5$ and radial velocities within $10\,000\text{ km s}^{-1}$. As a control sample for them we use a population of 722 more thick RFGC galaxies with $(a/b)_b > 7$, situated in the same volume. The UFG distribution over the sky indicates them as a population of quite isolated galaxies. We found that the specific star formation rate, $sSFR_{\text{FUV}}$, determined via the FUV GALEX flux, increases steadily from the early type to late type disks for both the UFG and RFGC–UFG samples, showing no significant mutual difference within each morphological type T . The population of UFG disks has the average H I-mass-to-stellar-mass ratio by (0.25 ± 0.03) dex higher than that of RFGC–UFG galaxies. Being compared with arbitrary orientated disks of the same type, the ultra-flat edge-on galaxies reveal that their total H I mass is hidden by self-absorption on the average by approximately 0.20 dex. We demonstrate that using the robust stellar mass estimate via $\langle B - K \rangle$ -color and galaxy type T for the thin disks, together with a nowadays accounting for internal extinction, yields their $sSFR$ quantities definitely lying below the limit of $-9.4\text{ dex (yr}^{-1})$. The collected observational data on UFG disks imply that their average star formation rate in the past has been approximately three times the current SFR . The UFG galaxies have also sufficient amount of gas to support their observed SFR over the following nearly 9 Gyrs.

1. INTRODUCTION

Since the time of the first studies [1, 2], star formation in galaxies is examined at the scales of the Local Volume (at the distances up to 10 Mpc [3–5]), of the nearby universe (approx-

imately up to 50 Mpc [6, 7]), as well as at $z \sim 1$, where the evolutionary effects become significant [8–10]. The methods determining the star formation rate (SFR) from radiation in the far and near ultraviolet ranges, in the $\text{H}\alpha$ line, from the equivalent widths of spectral lines, etc. were developed (see the survey [11]). Detailed optical and radio observations were conducted

* Electronic address: melnykol@gmail.com

** Electronic address: ikar@sao.ru

and SFR was determined for small samples of nearby galaxies (e.g., [12, 13]).

A massive study of star formation in the galaxies became possible owing to the emergence of large-scale sky surveys, carried out in ultraviolet, optical and infrared ranges: GALEX [14], SDSS [15], 2MASS [16, 17], WISE [18]. Advantages and disadvantages of determining the SFR in the most nearby (the possibility of individual approach) and distant galaxies (sample sizes of about tens of thousands of objects) are obvious.

A general conclusion from a vast array of publications (without touching the farthest objects) is that star formation in elliptical galaxies, not containing gas and dust, is quenched, while spiral and irregular dwarf galaxies demonstrate a high star formation rate, sufficient to explain the observed amount of their stellar mass.

For the galaxies of the nearby universe within $D \sim 50$ Mpc the upper limit of specific star formation rate was found, $\log sSFR = -9.4 \text{ yr}^{-1}$ [19–21]. This condition is met for the Local Volume galaxies ($D < 10$ Mpc), located in the environments of different density [19], as well as for the LOG [22] and 2MIG [23] catalogs of isolated galaxies, having the depth of $z \sim 0.01$.

The studies devoted to star formation in spiral galaxies usually consider the objects arbitrarily inclined to the line of sight [24]. Only a few authors have separately studied the highly inclined (edge-on) spirals (see [25] and the references therein).

Heidmann et al. [26] have earlier found that

namely the late-type spirals are characterized by the highest axial ratios a/b , where a and b are the major and minor angular diameters. As it was shown by Karachentsev [27], selection of galaxies based on their apparent axial ratio $a/b \geq 7$ allows to choose flat disks without noticeable signs of the bulge from an array of spirals. The application of this simple selection criterion led to the creation of flat galaxy catalogs: Flat Galaxy Catalog (FGC [28]) and its improved version, the Revised Flat Galaxy Catalog (RFGC [29]) covering the entire sky.

Apart from the morphological features, flat late-type spirals have other peculiarities. Firstly, they are distributed over the sky quite homogeneously, without any visible clumps in the areas occupied by clusters of galaxies [28]. A more detailed examination has shown that about 60% of ultra-flat edge-on galaxies are isolated, while about 30% belong to diffuse associations of galaxies, and only 10% have nearby, physically bound neighbors [30, 31]. It can therefore be assumed that star formation in these objects is mainly due to the internal processes, not being affected by nearby neighbors. Secondly, late spirals are characterized by a high degree of detection in the HI 21 cm line. This allows to determine their maximum amplitude of rotation V_m with a good accuracy, which is used in particular to account for the internal extinction of light.

Note that the systematic study of star formation in the RFGC spiral galaxies was made possible with the advent of the GALEX ultravi-

olet sky survey [14]. The purpose of the present study is to compare the SFR in ultra-flat and flat edge-on galaxies. Both samples were taken from the RFGC catalog. Special attention is given to different methods of estimation of the internal extinction A^i and determining the integral stellar mass of the galaxy M_* .

Section 2 describes the samples of flat and ultra-flat galaxies. Section 3 discusses the ways of accounting for the internal extinction in edge-on galaxies. Section 4 briefly describes the features of determination of the FUV flux and SFR. Section 5 is devoted to different ways of estimation of the stellar mass of galaxies, and selecting the most optimal of them. Section 6 presents our main findings. Discussion and conclusions are given in Section 7.

2. ORIGINAL DATA FOR ULTRA-FLAT GALAXIES

The RFGC catalog [29] contains $N = 4236$ galaxies with angular diameters $a \geq 0.6$ and apparent axial ratios $a/b \geq 7$ on the blue images of the First Palomar Sky survey. From the RFGC catalog we have selected ultra-flat galaxies (UFG, $N = 817$), for which the mutual conditions for the “blue” and “red” axial ratios were met: $(a/b)_{\text{blue}} \geq 10$, $(a/b)_{\text{red}} \geq 8.5$. To reduce the impact of the selection effects, we added restrictions on the angular diameter, Galactic latitude and radial velocity: $a_{\text{blue}} \geq 1.0$, $|b| > 10^\circ$, $V_h < 10\,000 \text{ km s}^{-1}$. The number of thin UF

galaxies amounted to $N = 441$.

The application of the Schmidt test has shown that the completeness of the RFGC catalog at $a_{\text{blue}} \geq 1.0$ is 70%, and the completeness of about 90% is achieved at the angular diameter of $a_{\text{blue}} = 1.2$ [29]. We have strengthened the selection criteria to ensure the acceptable completeness (90%), reduce the selection effects, and at the same time to have a rather large number of galaxies remaining. Flat galaxies with the following characteristics were selected from the RFGC catalog: ‘ $a_{\text{blue}} \geq 1.2$, $(a/b)_{\text{blue}} \geq 7$, $|b| > 10^\circ$, $V_h < 10\,000 \text{ km s}^{-1}$.

Some galaxies have been excluded from the consideration based on the following:

- 1) poor photometry due to a projected bright star (cases of RFGC 514, 1543, 1747 and 3830);
- 2) a discrepancy between the direct distance estimate and the distance determined from radial velocity, RFGC 384, 2239 and 2246;
- 3) galaxy RFGC 2614 was included in the sample by mistake (in the LEDA database it is given $V_h = 11\,354 \text{ km s}^{-1}$).

Therefore, in our truncated RFGC catalog sample (further in this paper this sample is referred to as the RFGC sample) $N = 1055$ flat galaxies are remaining. Among them, the population of ultra-flat galaxies (UFG) numbers $N = 333$ objects.

The following RFGC catalog [29] data were used: equatorial coordinates of galaxies, their “blue” and “red” axial ratios a/b , and morphologi-

cal types. From the NED¹ and HyperLEDA² [32] databases the heliocentric radial velocities V_h were taken and converted to V_{LG} , according to [33]. From the HyperLEDA we have also adopted the values of the apparent total magnitude B_t (for 1055 RFGC objects and 333 UFG objects), the maximum rotation velocity V_m (979 and 311) and the magnitude in the 21 cm line m_{21} (831 and 258). The g , r , i magnitudes at $0 < g - r < 1.1$ (448 and 156) were taken from the SDSS (DR13) survey, while from the 2MASS survey we took the K_s values (837 and 235), and from the WISE—the magnitudes for 988 and 301 galaxies, respectively. The magnitudes in the latter three surveys were determined in the AB system.

Figure 1 shows the sky distribution in the equatorial coordinates of the selected flat $N = 1055$ (top panel) and ultra-flat galaxies $N = 333$ (bottom panel). Galaxies possessing radial velocities $V_{LG} < 3500 \text{ km s}^{-1}$ are marked with larger symbols. The region with the Galactic latitude $|b| < 10^\circ$ is painted gray. There is a weak concentration of nearby flat galaxies along the equator of the Local Supercluster and in the region of the nearby scattered cloud in Canes Venatici. The effect is almost not noticeable for ultra-flat galaxies, what indicates a higher fraction of isolated galaxies among them.

Figure 2 presents a general understanding of the distribution of the main observed character-

istics. On each panel there, ultra-flat galaxies are marked with black color. As seen from the distribution based on radial velocity, the sample of UFG galaxies has approximately the same depth as the sample of RFGC galaxies. Consequently, the effect of the galaxy selection based on luminosity does not play a significant role in the comparison of properties of UFG and RFGC populations.

The distribution of RFGC galaxies based on morphological types has a peak for the Sc–Scd types ($T = 5\text{--}6$), while in the UFG galaxies the peak is shifted to a later type Sd ($T = 7$). This once again emphasizes the well-known fact that the thinnest disks are typical of galaxies, the spiral structure of which is on the verge of transition from a regular to chaotic pattern.

As shown in Fig. 2c, the considered RFGC galaxy sample of galaxies has a photometric completeness to the apparent magnitude of $B_t \simeq 16^m0$. For the UFG galaxies the completeness limit is shifted by $\Delta B \simeq +0^m5$, and the systematic difference is preserved within each morphological type.

Figure 2d indicates that in the photometric K_s -band of the 2MASS survey both samples start losing their completeness at $K_s \simeq 12^m0$. For many flat galaxies having a bluish color and low surface brightness, 2MASS-photometry at $K_s > 12^m0$ proves to be burdened with significant systematic errors.

Table 1 lists the mean values and errors in mean for the observed characteristics of UFG

¹ <http://nedwww.ipac.caltech.edu>

² <http://leda.univ-lyon1.fr>

Table 1. Average values and standard errors of the mean for the original characteristics of the flat and ultra-flat galaxies depending on the morphological type

Parameter	Morphological type						
	All types	2 + 3	4	5	6	7	8 + 9
$(a/b)_b$	$N_{\text{RFGC-UFG}} = 722$	67	170	201	143	67	74
	8.53 ± 0.04	8.15 ± 0.14	8.35 ± 0.07	8.62 ± 0.09	8.87 ± 0.10	8.68 ± 0.14	8.24 ± 0.12
	$N_{\text{UFG}} = 333$	8	16	70	80	134	25
	12.74 ± 0.13	10.33 ± 0.08	11.60 ± 0.33	12.32 ± 0.23	12.51 ± 0.24	13.50 ± 0.24	12.04 ± 0.35
$(a/b)_r$	$N_{\text{RFGC-UFG}} = 722$	67	170	201	143	67	74
	7.54 ± 0.04	6.91 ± 0.14	7.21 ± 0.07	7.69 ± 0.07	8.01 ± 0.12	7.72 ± 0.15	7.34 ± 0.12
	$N_{\text{UFG}} = 333$	8	16	70	80	134	25
	11.27 ± 0.11	9.19 ± 0.31	9.99 ± 0.31	10.55 ± 0.16	11.05 ± 0.19	11.98 ± 0.18	11.59 ± 0.52
B_t	$N_{\text{RFGC-UFG}} = 722$	67	170	201	143	67	74
	15.40 ± 0.03	15.22 ± 0.11	15.39 ± 0.07	15.48 ± 0.06	15.32 ± 0.10	15.45 ± 0.13	15.49 ± 0.11
	$N_{\text{UFG}} = 333$	8	16	70	80	134	25
	15.92 ± 0.04	15.61 ± 0.23	15.99 ± 0.13	15.88 ± 0.08	15.93 ± 0.07	15.98 ± 0.06	15.77 ± 0.18
K_s	$N_{\text{RFGC-UFG}} = 602$	65	167	181	118	45	26
	11.25 ± 0.05	10.70 ± 0.13	11.06 ± 0.08	11.33 ± 0.08	11.47 ± 0.13	11.52 ± 0.16	11.82 ± 0.27
	$N_{\text{UFG}} = 235$	8	12	56	63	87	9
	11.96 ± 0.06	11.75 ± 0.37	11.29 ± 0.24	11.65 ± 0.15	12.02 ± 0.12	12.23 ± 0.13	12.00 ± 0.41
V_{LG}	$N_{\text{RFGC-UFG}} = 722$	67	170	201	143	67	74
	4708 ± 92	5591 ± 278	5832 ± 181	5285 ± 168	3920 ± 166	3365 ± 240	2498 ± 207
	$N_{\text{UFG}} = 333$	8	16	70	80	134	25
	5057 ± 127	5128 ± 758	7071 ± 397	5467 ± 243	5730 ± 274	4644 ± 179	2660 ± 400
V_m	$N_{\text{RFGC-UFG}} = 722$	67	170	201	143	67	74
	145 ± 2	184 ± 6	178 ± 4	154 ± 4	124 ± 3	108 ± 4	81 ± 5
	$N_{\text{UFG}} = 333$	8	16	70	80	134	25
	131 ± 3	154 ± 24	185 ± 12	150 ± 6	139 ± 6	118 ± 3	84 ± 6
$g - r$	$N_{\text{RFGC-UFG}} = 306$	19	84	97	51	23	32
	0.72 ± 0.03	0.83 ± 0.03	0.77 ± 0.02	0.70 ± 0.02	0.60 ± 0.02	0.51 ± 0.07	0.41 ± 0.10
	$N_{\text{UFG}} = 149$	0	3	30	40	69	7
	0.64 ± 0.02	–	0.95 ± 0.01	0.80 ± 0.02	0.60 ± 0.04	0.57 ± 0.03	0.42 ± 0.16
$W2-W4$	$N_{\text{RFGC-UFG}} = 687$	67	169	196	135	59	61
	5.11 ± 0.03	4.42 ± 0.12	4.81 ± 0.06	5.16 ± 0.05	5.34 ± 0.05	5.43 ± 0.07	5.71 ± 0.08
	$N_{\text{UFG}} = 301$	7	15	64	78	118	19
	5.16 ± 0.04	5.03 ± 0.61	4.77 ± 0.18	4.93 ± 0.09	5.17 ± 0.06	5.26 ± 0.05	5.64 ± 0.13

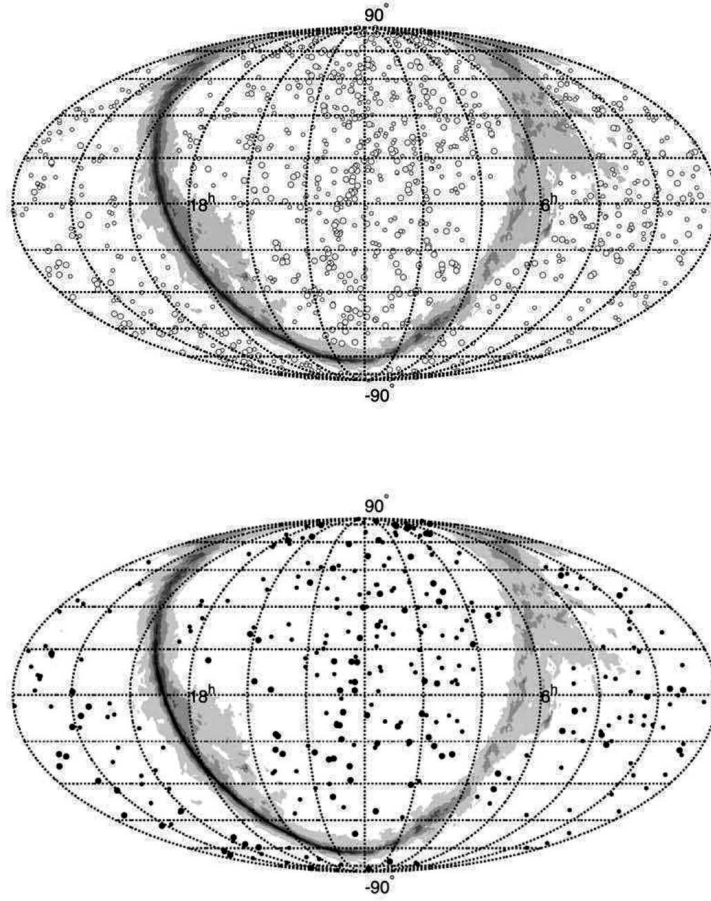


Figure 1. The sky distribution in equatorial coordinates of the flat galaxies RFGC, $N = 1055$ (empty circles), and ultra-flat UFG, $N = 333$ (filled circles). Gray fill marks the area of strong Galactic extinction $|b| < 10^\circ$. Large circles mark the galaxies with $V_{LG} < 3500 \text{ km s}^{-1}$, and small circles—with $V_{LG} = 3500 - 10000 \text{ km s}^{-1}$.

and RFGC–UFG galaxies depending on the type. The bottom line corresponds to ultra-flat galaxies, while the top line lists flat galaxies. The few cases of $T = 2$ and $T = 9$ are respectively combined with the $T = 3$ and $T = 8$ types. From a comparison of the data presented the following conclusions can be made.

- The mean apparent axial ratio shows the expected increase from the early-type to late-type spirals. The peak of the distribution for UFG

galaxies both in the blue and in the red bands falls on $T = 7$, whereas for RFGC–UFG galaxies the maximum is fixed at $T = 6$.

- Among all the morphological types, ultra-flat galaxies look somewhat fainter than simply flat galaxies (RFGC–UFG). The mean difference in the apparent magnitudes amounts to $+0^m52 \pm 0^m05$ in the B -band and $+0^m71 \pm 0^m08$ in the K_s -band. The reason for this difference could be internal extinction in strongly in-

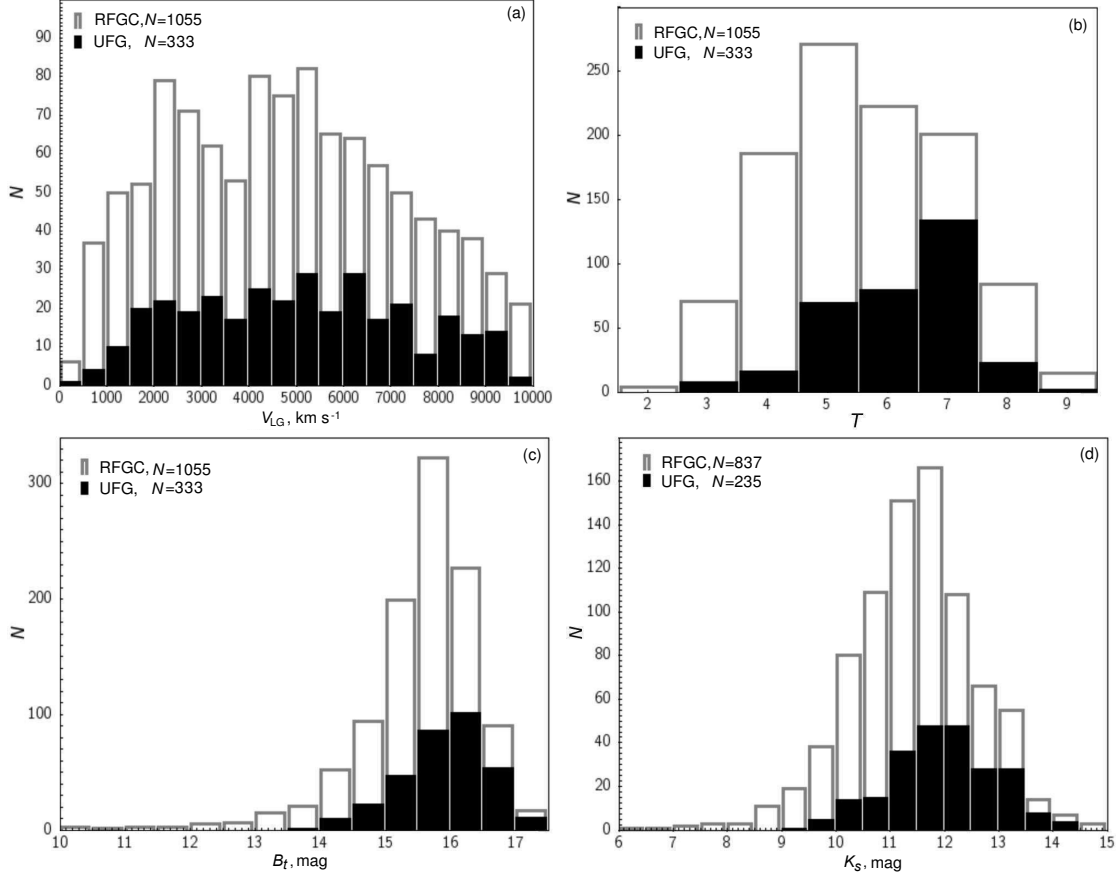


Figure 2. Histograms of the distribution of the number of galaxies based on the observed characteristics: (a) radial velocity V_{LG} ; (b) morphological type T ; (c) the apparent total magnitude B_t from the HyperLEDA database; (d) the 2MASS survey K_s magnitude. The data relating to ultra-flat galaxies, UFG, are darkened.

clined disks. However, then the difference in the infrared band would be significantly smaller than in the blue band. A more likely cause is hidden selection effects due to methodological features of the photometry of extended low-contrast galaxy images.

- The average radial velocity (i.e., distance) of ultra-flat galaxies does not differ much from the average for the RFGC–UFG-objects. Also, a small difference is found for the mean rotation amplitude V_m , which is closely correlated with the luminosity of the galaxy. In other words,

both samples refer to about the same volume of space.

- A significant portion of studied objects lie in the zone of the SDSS survey (DR13), what allows to compare their average optical color indices $\langle g - r \rangle$. According to the table data, the color differences of UFG and RFGC–UFG galaxies are small, which does not impose any restriction on the nature of internal extinction in thin disks.
- More than 90% of RFGC galaxies are detected in four infrared bands of the WISE sky sur-

vey [18]: $W1$, $W2$, $W3$, $W4$ ($3.38\ \mu\text{m}$, $4.6\ \mu\text{m}$, $12.33\ \mu\text{m}$ and $22.00\ \mu\text{m}$). Here the most long-wavelength band is the most sensitive to the thermal flux of dust, re-emitting the total stellar flux. The $W4$ value is an additional indicator of the amount of dust and integral SFR in a galaxy. As can be seen from the average values of $\langle W2 - W4 \rangle$, the color index increases steadily from the early to late morphological types. Between the values of $\langle W2 - W4 \rangle$ in general, no significant differences were observed in the UFG and RFGC–UFG galaxies. However, within each morphological type ultra-flat galaxies look somewhat more “blue” (less dusty) than the others.

3. ACCOUNTING FOR INTERNAL EXTINCTION IN SPIRAL GALAXIES

The presence of dust in the disk of a spiral galaxy reduces its integral luminosity. The internal extinction effect is the most strongly manifested in edge-on galaxies, and grows from the infrared to ultraviolet spectral regions. The distribution of bright blue stars and dust clouds in the disk of a spiral galaxy is extremely uneven and can not be described by a simple model of plane-parallel layers. Therefore, so far there is no reliable and universal scheme of accounting for internal extinction.

The formulation of the corrections to the apparent magnitude of a galaxy for its inclination, adopted in various editions of The Reference Cat-

alogue of Galaxies (see, e.g., [34]) and in the HyperLEDA, changed over time. Its main drawback was that it ignored the dependence of the extinction magnitude on the luminosity of a spiral galaxy, to what Tully et al. [35] and Verheijen and Sancisi [36] have paid due attention. According to [36], weakening of the integral magnitude of galaxies in the B -band is expressed by:

$$A_B^i = [1.54 + 2.54(\log V_m - 2.2)] \log(a/b) \quad (1)$$

for $V_m > 43\ \text{km s}^{-1}$, where a/b is the apparent axial ratio, and V_m is the amplitude of rotation in km s^{-1} ; $A_B^i = 0$ for $V_m < 43\ \text{km s}^{-1}$. According to (1), the extinction steadily increases with increasing V_m or luminosity. Basically this formula reasonably describes internal extinction in spiral galaxies, giving on the average a lower correction for the extinction than the RC3 and LEDA.

In their recent publication [37] Devour and Bell examined the integral features of 78 720 SDSS galaxies with redshifts $z < 0.1$ and apparent red magnitudes $m_r < 17^m7$. Comparing different ways of accounting for internal extinction, the authors came to the conclusion that the schemes of corrections for the inclination, proposed in [35] and [38] overestimate the extinction for the brightest galaxies. According to [37], internal extinction increases with increasing luminosity of a spiral galaxy not monotonely, but has a peak at the maximum absolute magnitude $M_K = -21.7$. Based on the data of Fig. 12 from [37], we found that the value of internal extinction in the B -band for a spi-

ral galaxy with the absolute magnitude M_K at $H_0 = 73 \text{ km s}^{-1} \text{ Mpc}^{-1}$ can be represented by a parabolic relation

$$A_B^i = [0.80 - 0.0584(M_K^{\text{corr}} + 21.7)^2] \log(a/b)_r, \quad (2)$$

where $(a/b)_r$ is the apparent axial ratio of the galaxy measured in the RFGC catalog at the red images of the Palomar Observatory Sky Atlas. Expression (2) is applicable to the range of $-17.7 > M_K > -25.7$, and outside of it the negative values of A^i are replaced by zero. For example, for the SMC dwarf galaxy with $M_K = -18.8$, $V_m = 46 \text{ km s}^{-1}$ and $(a/b) = 1.56$, relationships (1) and (2) give similar values: $A^i = 0^{\text{m}}03$ and $0^{\text{m}}06$ respectively. However, for an ultra-flat galaxy with $(a/b) = 10$, $V_m = 200 \text{ km s}^{-1}$ and $M_K = -24.2$ the difference of the corrections for A^i becomes significant: $1^{\text{m}}80$ and $0^{\text{m}}44$. Here for the transition from V_m to M_K we used the calibration ratio from [35]

$$M_K^{\text{corr}} = -23.29 - 8.78 (\log V_m - 2.20). \quad (3)$$

At that, the range of positive values of the A^i correction corresponds to the V_m interval from 39 km s^{-1} to 300 km s^{-1} .

The amplitude of rotation V_m , which we adopted from the HyperLEDA, is now known for 85% of the RFGC galaxies. In the absence of the data on V_m we calculated this value from the empirical regression between V_m (km s^{-1}) and the morphological type of a given galaxy:

$$V_m = -20.36 T + 254. \quad (4)$$

We made the recalculation of the correction for the internal A_B^i and external (Galactic) extinction A^G from the B -band to the FUV, K_s and $W1$ -bands using the relations:

$$\begin{aligned} A_{\text{FUV}}^t &= 1.930 (A_B^i + A^G), \\ A_{K_s}^t &= 0.083 (A_B^i + A^G), \\ A_{W1}^t &= 0.052 (A_B^i + A^G), \end{aligned} \quad (5)$$

where the parabolic dependence (2) was used to take into account the internal extinction.

4. FUV FLUXES AND SFR

We expressed the integral SFR of a galaxy through its apparent magnitude in the FUV-band, corrected for the extinction as in [21]:

$$\log SFR = 2.78 - 0.4 m_{c, \text{FUV}} + 2 \log D, \quad (6)$$

where the distance $D = V_{\text{LG}}/73$ is expressed in Mpc, and SFR —in $M_{\odot} \text{ yr}^{-1}$. According to [11, 39], this relation fixes the SFR at the characteristic timescale of about 10^8 yrs determined by the radiation of young blue stars.

The sky survey made with the GALEX Space Telescope [14], registered the FUV-fluxes for approximately 75% of galaxies in our sample. In the softer NUV-range the percentage is slightly higher (84%), but we will further restrict to using only the FUV-magnitudes, as we did in our previous papers [19–21]. The images of thin spiral disks in the FUV and NUV-bands look low-contrast and shredded, often breaking into a chain of separate condensations with individual m_{FUV} and m_{NUV} estimates. Determining the

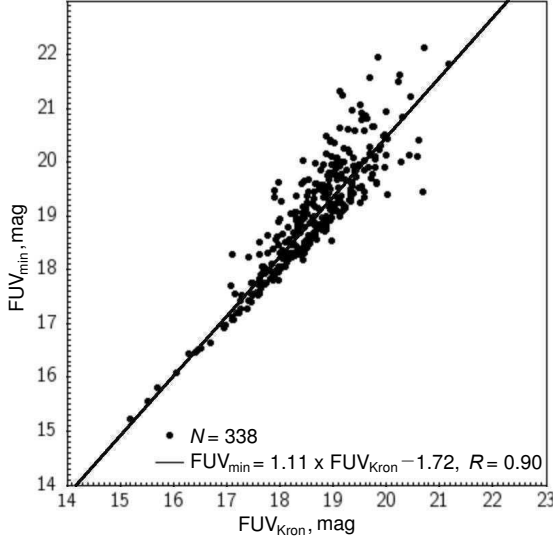


Figure 3. A comparison of the of the FUV photometry data in the elliptical Kron and circular apertures. The figure shows the regression parameters.

SFR in a galaxy we focused on the values of Kron elliptical aperture magnitudes, which are available for almost half of the objects of our sample. For the rest, we used the so-called m_{\min} , corresponding to the FUV-flux from the brightest concentration in the galaxy. This technique allowed to avoid the manual analysis of numerous individual images having a low angular resolution (about $5''$) and low contrast. The distribution of our galaxies by the FUV-magnitudes m_{Kron} and m_{\min} is shown in Fig. 3. The relation between them is described by a regression

$$m_{\text{FUV, Kron}} = 0.9 m_{\text{FUV, min}} + 1.55 \quad (7)$$

with the correlation coefficient $R = 0.90$. On the average the transition from m_{\min} to m_{Kron} required a correction by about $-0^{\text{m}}.4$ at the typical dispersion of around $0^{\text{m}}.5$. Further in the paper we use Kron’s FUV-magnitudes directly

measured in the elliptic apertures or recomputed from m_{\min} by relation (7). Thus, the integral SFR was determined by relation (6) accounting for the corrections (2) and (5).

It is known that the integral SFR of a galaxy quite closely correlates with its total stellar mass, forming the so-called “main sequence” on the $\log SFR \propto \log M_*$ diagram. Therefore, further for each galaxy in our sample, we determined its stellar mass using different approaches.

5. GALAXY STELLAR MASS ESTIMATION

Integral stellar mass of a galaxy M_* is usually determined by the spectral energy distribution (SED), specifying a particular shape of the initial stellar mass function (IMF) by Salpeter [40], Kroupa [41] or Chabrier [42]. In practice, M_* is more frequently estimated using integral luminosity of a galaxy in certain band, taking a fixed mass-to-luminosity ratio. We calculated the stellar mass from the galaxy K -band luminosity at the value of $M_*/L_K = 1(M_\odot/L_\odot)$ [43] and $M_{\odot, K} = 3^{\text{m}}.28$ [44]. As noted in [45], the M_*/L_K relation has not yet been fixed very reliably and most likely lies in the range of $[0.5 - 1.0]M_\odot/L_\odot$.

The apparent K -magnitude of the galaxy can be determined in several ways.

- 1) The infrared survey the entire sky 2MASS [16] contains automatic evaluations of K_s -magnitudes for 73% of galaxies in our sample. However, due to short exposures (approximately 8 s) the survey is insensitive

to bluish structures of low surface brightness. As a result of underestimation of the real size of thin disks and their frequent separation into a few fragments, the integral K_s -fluxes of many RFGC galaxies are systematically underestimated, particularly for faint galaxies with $K_s > 12^m$.

2) The WISE infrared sky survey [18] has the magnitude estimates in four infrared bands: $W1$, $W2$, $W3$ and $W4$ for 94% galaxies under consideration. This survey, as well as 2MASS suffers from the flux underestimation from the periphery of diffuse galaxies. The apparent magnitude of RFGC galaxies in the $W1$ band, closest to K_s , shows a tight correlation with K_s ; the ratio between them has the form

$$K_s = 0.99 K_{W1}^c - 0.06, \quad (8)$$

where $K_{W1}^c = m_{W1} - 0.83$, the correlation coefficient $R = 0.90$, the number of galaxies $N = 813$. This K_s -magnitude, derived from the $W1$ -magnitude shall be further referred to as K_W .

3) According to [46], the mean color index of the galaxy depends on its morphological type as

$$\langle B - K \rangle_{\text{corr}} = 4.60 - 0.25 T \quad (9)$$

at $T = 2, 3, \dots, 9$. Using this relation and taking into account the corrections for the extinction (2) and (5), we determined the K -magnitudes for all the RFGC galaxies. These

values will be further denoted as K_B . The regression line for them and the K_s -magnitude, constructed from 837 galaxies, has the form

$$K_s = 0.56 K_B + 4.87. \quad (10)$$

4) We can also estimate the absolute K -magnitude from the calibration relation (3) considering the additional relation (4) for the galaxies without direct V_m measurements.

Two-dimensional distributions of galaxies from our sample based on $\{K_s, K_W\}$, $\{K_s, K_B\}$ and $\{K_W, K_B\}$ are shown in three panels of Fig. 4. The solid and dashed lines denote the regression line and the diagonal, respectively. Apart from the main array of galaxies, each panel contains about 1% of cases with large deviations from the regression line. In Fig. 4 such objects are outlined by squares. Additional analysis shows that the main reasons for these deviations are the infrared photometry errors, when there is a loss of flux the periphery of a given galaxy (the cases of RFGC 566, 1295, 2245, 2315, 2335, 3854), or a bright star is projected on the galaxy (RFGC 668, 1049, 1340, 2140, 3357). In our experience, the most reliable measurement of stellar mass in thin spiral edge-on galaxies is to use the K_B -magnitude.

6. SPECIFIC AND EFFECTIVE SFR

Dependences of the specific star formation rate $sSFR = SFR/M_*$ on the morphological

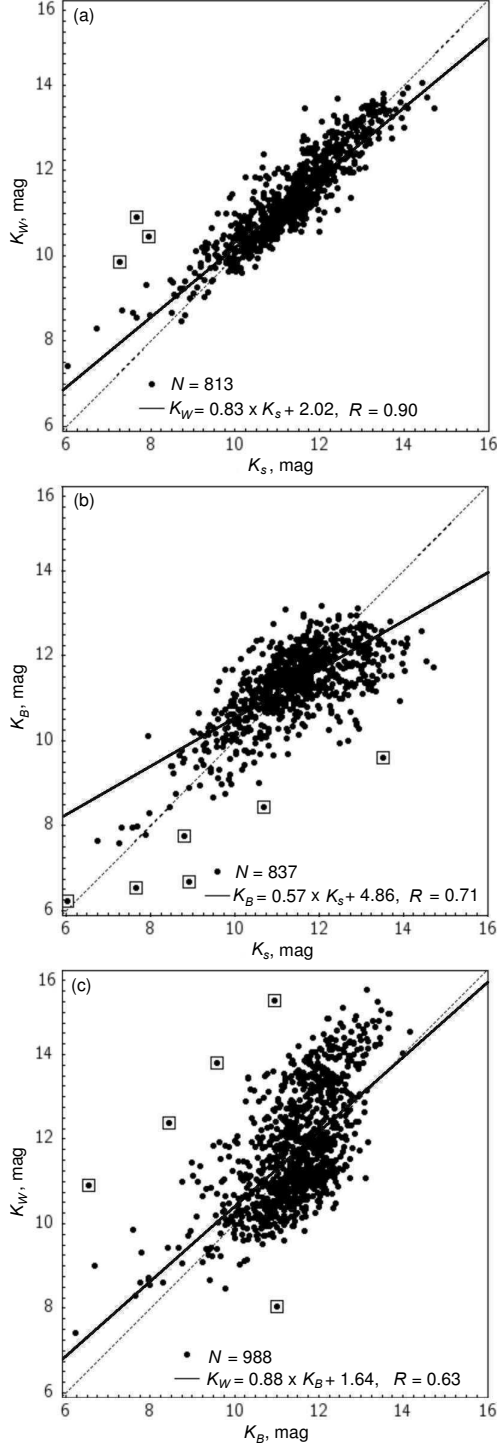


Figure 4. Mutual dependences of the calculated and observed magnitudes for flat and ultra-flat galaxies (from top to bottom): K_W vs K_S ; K_B vs K_S ; K_W vs K_B . The figures show the corresponding regression parameters and the number of galaxies. The squares outline the objects strongly diverging from the regression line.

type of the galaxy T for the UFG (dark circles) and RFGC–UFG (gray circles) disks are presented in four panels of Fig. 5. Stellar mass was identified with the K -luminosity ($M_* = L_K$), and K -magnitudes were determined in four variants described above. For a better visualization, the data for the UFG sample are shifted to the right on the horizontal axis. The corresponding number of galaxies is indicated in the corner of each panel.

As might be expected, specific SFR on the average increases from early to late spirals. However, comparing the diagrams we can see that the most clear dependence $\log sSFR$ on the type manifests itself when K_B -magnitude is used to determine the stellar mass. No specific differences in the $sSFR$ between the UFG and RFGC–UFG galaxies are observed.

Figure 6 represents the $\log sSFR$ dependence on the stellar mass for the four K -luminosity estimation alternatives. The designations of flat and ultra-flat galaxies are the same as in the previous figure. To properly compare the data of different panels, we presented there only 178 UFG galaxies and 428 RFGC–UFG galaxies, for which the K -magnitude estimates are available by all four methods. The horizontal line in all panels corresponds to the value of $\log sSFR = -9.4$ we marked earlier [19–21] as a certain quasi-“Eddington” limit for the star formation intensity at the present epoch. Above this limit there are only a few galaxies, the K -luminosity (stellar mass) of which is underestimated from the

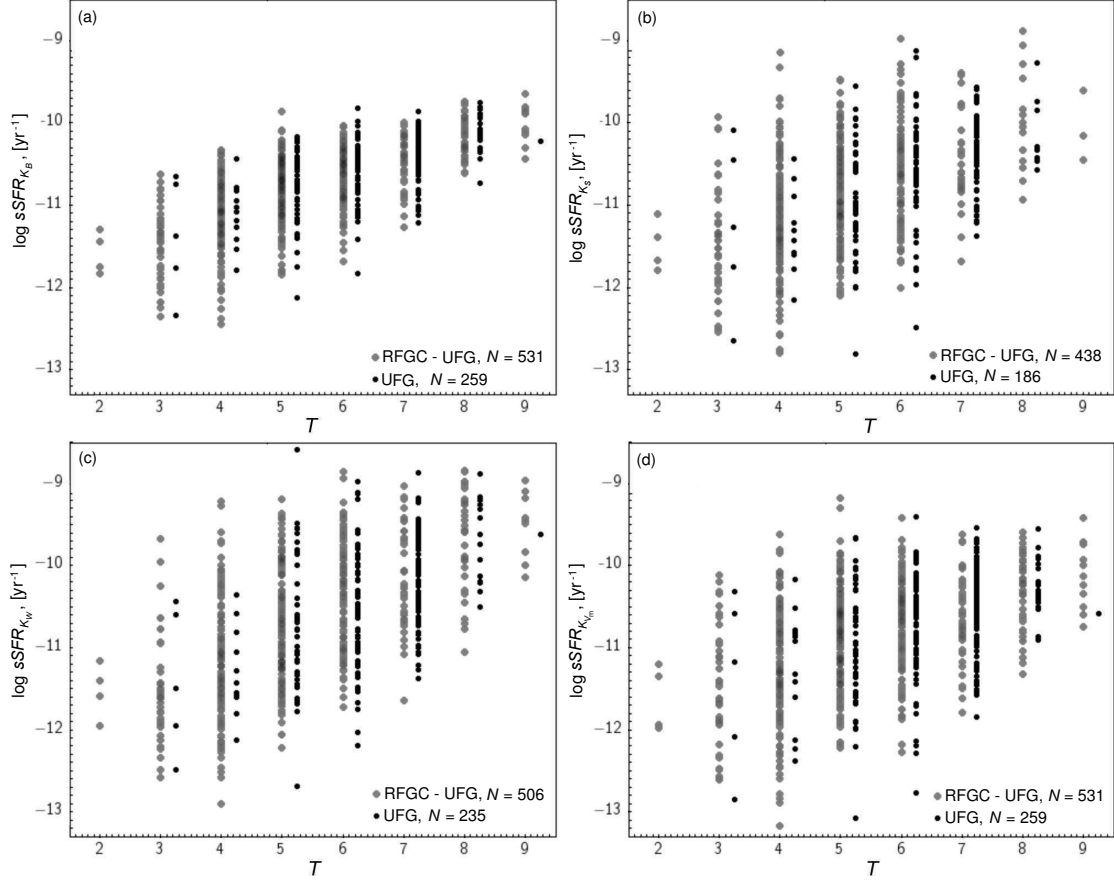


Figure 5. The dependence of specific star formation rate $\log sSFR$ on the morphological type of the galaxy T for RFGC–UFG and UFG galaxies—gray and dark circles respectively. Stellar mass of the galaxy was determined from its K -luminosity at $M_* = 1M_\odot/L_\odot$. The K -magnitudes of galaxies were evaluated in four different ways: K_B —from the B -magnitude and morphological type, K_s —according to the 2MASS-survey, K_w —from the $W1$ -magnitude of the WISE-survey, K_{V_m} —from relation (3) between the rotation amplitude V_m and absolute K -magnitude.

infrared photometry.

As it can be seen, the behavior of dependences for flat and ultra-flat galaxies is approximately the same. It should be noted that the stellar mass of the galaxy is present on both scales of Fig. 6 panels, therefore the inevitable errors in the M_* due to unreliable photometry (sometimes reaching the order of magnitude) stretch the observed distribution cornerwise $\Delta \log sSFR = -\Delta \log M_*$. This is why the

maximal $sSFR$ values prove to be in galaxies with a minimal mass estimate. Figure 6 once again demonstrates that the smallest scatter of $sSFR$ estimates is typical for the case when the B -band photometry is used. Further on, from four ways of determining the K -magnitude for RFGC galaxies we would prefer the B -band photometry.

Some authors (see [47] and the literature cited there) use not only the spe-

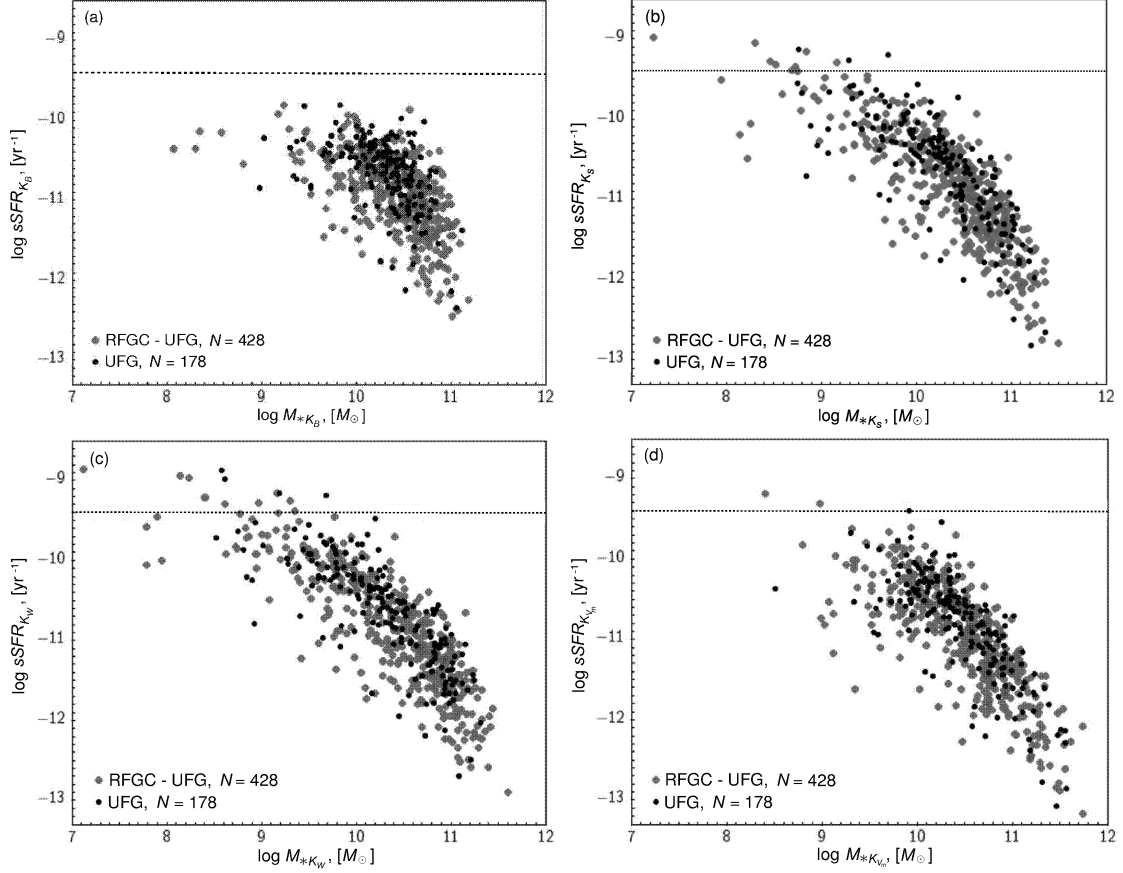


Figure 6. The specific SFR, depending on the luminosity (stellar mass) of the galaxy. Gray circles on the panels depict the RFG–UFG subsample galaxies ($N = 428$), and the dark circles—UFG galaxies ($N = 178$).

Luminosity (stellar mass) was determined in four ways, analogous to those in Fig.5.

cific, but also the effective star formation rate, $SFR_{\text{eff}} = \log(SFR/M_{\text{HI}})$, to characterize a galaxy. Here the hydrogen mass $M_{\text{HI}} = 2.356 \times 10^5 D^2 F_{\text{HI}}$ is expressed in solar mass units [48], D is the distance in Mpc, and F_{HI} is the flux in Jy km s^{-1} , calculated as $\log F_{\text{HI}} = 0.4(17.4 - m_{21})$. Figure 7 shows the dependence of the effective SFR on the stellar (the bottom panel) and hydrogen mass of galaxies. Both diagrams for SFR_{eff} look noticeably more diffuse than the diagrams for $sSFR$. The distributions of ultra-flat and flat galaxies do not show any particular mutual differences.

Integral flux of a galaxy in the infrared band $W4$ ($22.0 \mu\text{m}$) is the FUV-flux-independent SFR indicator. This is especially important for ultra-flat galaxies due to significant internal extinction in the ultraviolet. According to [49], the total star formation rate SFR_{tot} is expressed by

$$SFR_{\text{tot}} = SFR_{\text{FUV}} + 0.83 SFR_{\text{IR}}. \quad (11)$$

The dependence of specific total star formation rate $\log sSFR_{\text{tot}}$ on the stellar mass for ultra-flat and flat galaxies is shown in the diagram of Fig. 8a. Here the stellar mass was calculated from the K -luminosity determined via re-

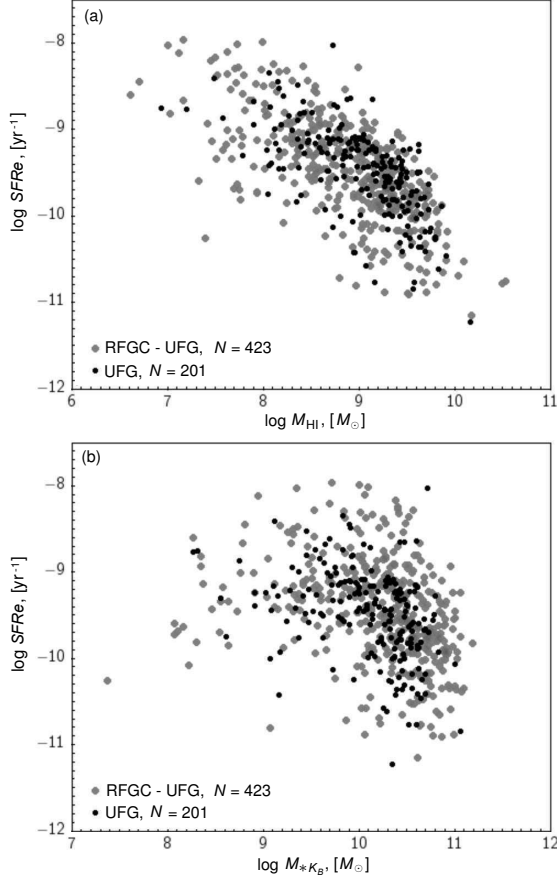


Figure 7. The effective SFR as a function of (a) hydrogen and (b) stellar mass of a galaxy.

Stellar masses were determined from the apparent total magnitude B_t (see Section 5).

lation (9). Unlike Fig. 6, this panel shows all UFG and RFGC–UFG galaxies with the SFR_{tot} estimates. Figure 8b shows the dependence of $sSFR_{\text{tot}}$ on the hydrogen-to-stellar-mass ratio of the galaxy. The population of UFG galaxies on it looks much more compact than that of the remaining RFGC galaxies.

The contribution of the infrared component in relation (11) is on the average small. For ultra-flat disks it amounts to 0.10 ± 0.04 dex, and for RFGC–UFG galaxies this contribution is somewhat larger: 0.20 ± 0.03 dex. As can be seen

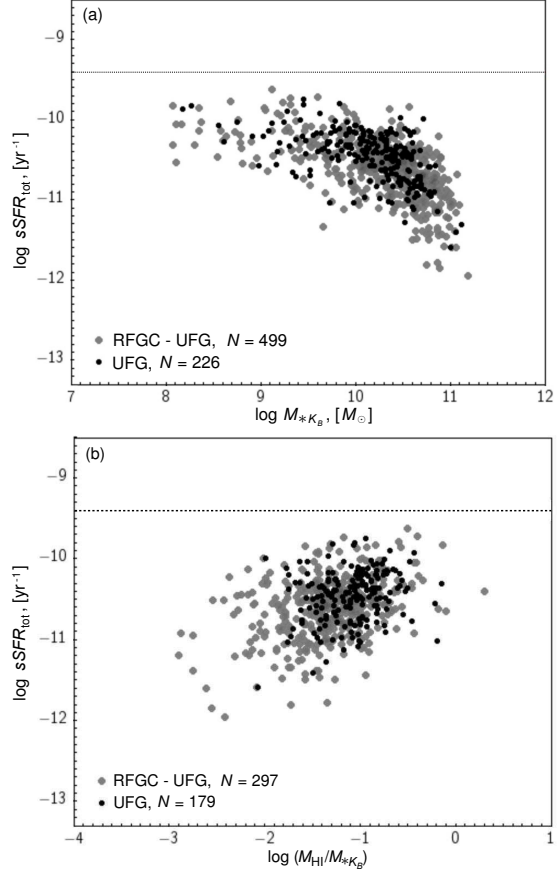


Figure 8. Full (FUV + IR) relative SFR depending on the stellar mass of the galaxy, determined from the K_s -luminosity via the apparent magnitude B_t (a) and depending on the value of the hydrogen-to-stellar mass ratio (b).

from the data presented in Fig. 9, the global SFR in the disks of flat galaxies, as well as the contribution to it of the IR component show a strong correlation with the morphological type. The average value of $\langle sSFR_{\text{tot}} \rangle$ monotonically increases by a magnitude from the $T = 2, 3$ types to $T = 8, 9$ types. At that, the ratio of SFRs, determined by equations (11) and (6), systematically drops from 0.4 dex for $T = 2 + 3$ to a virtually zero excess for the $T = 8 + 9$ types. The differences of ultra-flat and flat galaxies in both

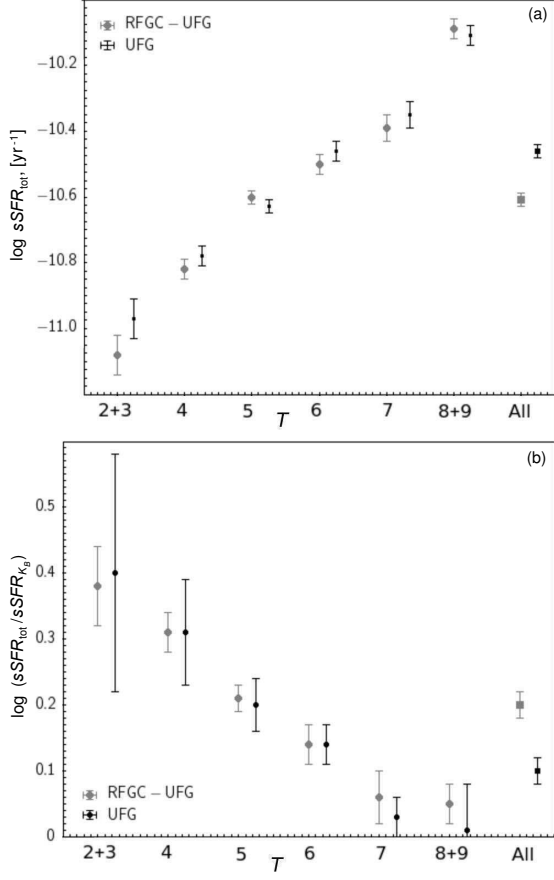


Figure 9. Top: full (from FUV + IR) relative SFR for ultra-flat and flat galaxies as a function of morphological type. Bottom: the ratio of specific SFR (full to the one determined from the FUV-flux) depending on the morphological type.

The last pairs of points on both panels are related to the averaged data for all types.

panels of Fig. 9 are within the random errors, but in general the UFG sample has a higher SFR due to the presence in it of a large fraction of late-type objects. Note that the account for the IR component in relation (11) leaves all the galaxies below the $\log sSFR = -9.4$ limit.

As noted by Karachentsev and Kaisin [50], the evolutionary status of a galaxy is convenient to characterize by dimensionless parameters P

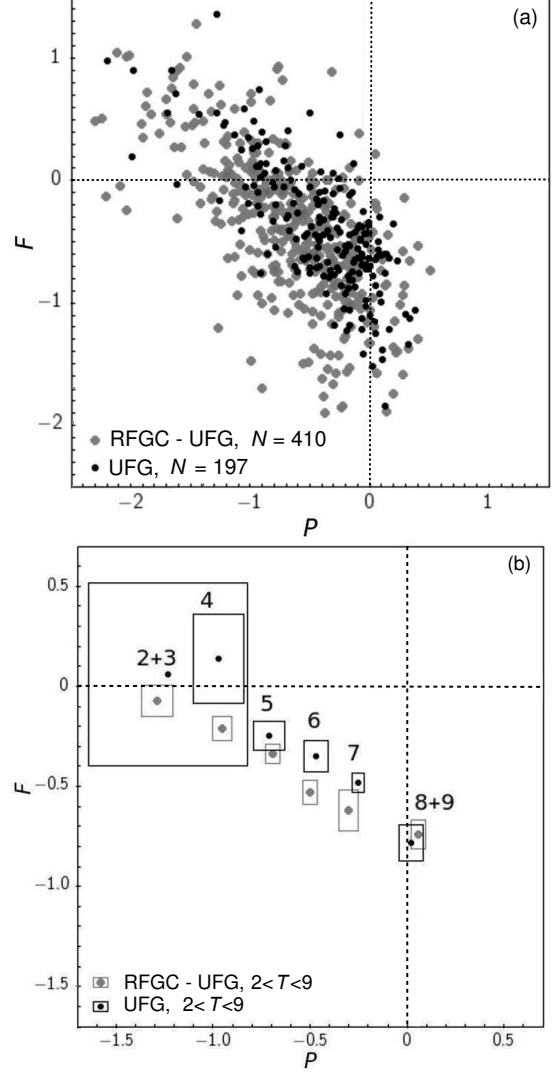


Figure 10. The diagnostic “Past-Future” diagrams for ultra-flat and flat galaxies: (a) the distribution of individual P and F values; (b) the mean P and F for different morphological types. The box sizes correspond to the errors in mean.

(Past) and F (Future), which do not depend on the distance:

$$P = \log(SFR \times T_0 / L_K), \quad (12)$$

$$F = \log[1.85 M_{H1} / (SFR \times T_0)]. \quad (13)$$

The P parameter expresses the specific star formation rate, normalized to the age of the Uni-

verse $T_0 = 13.7$ Gyrs. Parameter F (in the sense opposite to the effective SFR) shows how long the observed SFR can be maintained at the available gas reserves in the disk. The coefficient 1.85 at M_{HI} takes into account the contribution of helium and molecular hydrogen in the overall mass of gas [51].

Figure 10 represents a diagnostic “Past–Future” diagram for ultra-flat and flat galaxies. The top panel shows individual positions of each galaxy. The bottom panel demonstrates the mean values of the P and F parameters and their errors for different morphological types. As it can be seen, the overall distribution of galaxies at the P – F diagram is diagonally stretched, and disks of each morphological type are localized in a certain part of the diagram.

The mean values of various parameters, characterizing the masses and star formation rates in galaxies of different types are shown in Table 2. Its structure is the same as that of Table 1. Generally the differences of the mean parameters for the UFG and RFGC–UFG galaxies are small when compared within the same morphological type. However, the resulting differences between the two considered samples can be significant because of the different proportion in them of the early and late types of galaxies. The difference of UFG and RFGC–UFG disks is most noticeable based on the relative hydrogen abundance per stellar mass unit. On the average, this difference amounts to 0.25 ± 0.03 dex, somewhat varying from one morphological type to another.

From this result, distorted by the effects of observational selection in the least, it follows that the conversion of gas into stars in very thin disks happens with a noticeable delay compared with thicker disks.

7. FINAL REMARKS

The considered sample of ultra-flat galaxies is a population of spiral disks of the simplest structure, almost completely deprived of the spheroidal component (bulge). In modern models of galaxy formation it is assumed that such systems did not experience frequent mergers, residing in the areas of low number density of galaxies. For this reason, ultra-flat galaxies can serve as a reference sample for the study of the autonomous process of star formation, where the tidal interactions of neighbors are negligibly small. At the same time, however, it is possible that the process of accretion of intergalactic gas onto the thin disk has a significant impact on the evolution of isolated disks.

The diagnostic “Past–Future” diagram (Fig. 10) is the most obvious way to compare the evolutionary status of galaxies from various samples. As follows from the Table 2 data, the mean values of the P and F parameters for the ultra-flat galaxies amount to $\langle P \rangle = -0.43 \pm 0.03$ and $\langle F \rangle = -0.39 \pm 0.04$. For the remaining flat RFGC–UFG galaxies these parameters are somewhat different from the previous ones: $\langle P \rangle = -0.65 \pm 0.03$ and $\langle F \rangle = -0.39 \pm 0.03$.

Table 2. The mean values and the standard errors of the mean for the calculated characteristics of flat and ultra-flat galaxies depending on the morphological type

Parameter	Morphological type						
	All types	2+3	4	5	6	7	8+9
$\log SFR$	$N_{\text{RFGC-UFG}} = 531$	45	127	152	108	45	54
	-0.59 ± 0.02	-0.73 ± 0.05	-0.54 ± 0.04	-0.45 ± 0.03	-0.55 ± 0.05	-0.75 ± 0.09	-0.94 ± 0.09
	$N_{\text{UFG}} = 259$	5	12	52	66	102	22
$\log M_*$	-0.45 ± 0.03	-0.7 ± 0.29	-0.48 ± 0.11	-0.47 ± 0.05	-0.34 ± 0.05	-0.42 ± 0.04	-0.78 ± 0.14
	$N_{\text{RFGC-UFG}} = 722$	67	170	201	143	67	74
	10.26 ± 0.02	10.76 ± 0.04	10.6 ± 0.02	10.4 ± 0.03	10.1 ± 0.04	9.81 ± 0.07	9.33 ± 0.08
$\log M_{\text{HI}}$	$N_{\text{UFG}} = 333$	8	16	70	80	134	25
	10.12 ± 0.03	10.59 ± 0.12	10.62 ± 0.04	10.36 ± 0.04	10.24 ± 0.05	9.97 ± 0.04	9.32 ± 0.16
	$N_{\text{RFGC-UFG}} = 573$	51	132	160	120	54	56
$\log(M_{\text{HI}}/M_*)$	8.91 ± 0.03	9.09 ± 0.07	9.16 ± 0.05	9.09 ± 0.04	8.77 ± 0.06	8.61 ± 0.1	8.29 ± 0.08
	$N_{\text{UFG}} = 258$	7	12	55	62	102	20
	9.02 ± 0.03	9.01 ± 0.16	9.5 ± 0.09	9.15 ± 0.06	9.11 ± 0.06	8.98 ± 0.05	8.41 ± 0.14
$\log sSFR$	$N_{\text{RFGC-UFG}} = 573$	51	132	160	120	54	56
	-1.34 ± 0.02	-1.66 ± 0.06	-1.44 ± 0.04	-1.31 ± 0.03	-1.31 ± 0.05	-1.19 ± 0.07	-1.05 ± 0.07
	$N_{\text{UFG}} = 258$	7	12	55	62	102	20
$\log sSFR_t$	-1.09 ± 0.02	-1.51 ± 0.1	-1.11 ± 0.09	-1.22 ± 0.04	-1.08 ± 0.04	-1.00 ± 0.03	-1.06 ± 0.1
	$N_{\text{RFGC-UFG}} = 531$	45	127	152	108	45	54
	-10.81 ± 0.02	-11.46 ± 0.06	-11.13 ± 0.04	-10.81 ± 0.03	-10.64 ± 0.03	-10.45 ± 0.05	-10.14 ± 0.03
$\log SFR_e$	$N_{\text{UFG}} = 259$	5	12	52	66	102	22
	-10.56 ± 0.03	-11.37 ± 0.32	-11.09 ± 0.11	-10.83 ± 0.06	-10.6 ± 0.04	-10.38 ± 0.03	-10.12 ± 0.05
	$N_{\text{RFGC-UFG}} = 423$	35	97	122	92	37	40
P	-9.48 ± 0.03	-9.8 ± 0.08	-9.66 ± 0.06	-9.53 ± 0.05	-9.34 ± 0.06	-9.25 ± 0.1	-9.13 ± 0.07
	$N_{\text{UFG}} = 201$	4	9	43	48	79	18
	-9.48 ± 0.04	-9.93 ± 0.46	-10.01 ± 0.22	-9.62 ± 0.07	-9.52 ± 0.08	-9.39 ± 0.05	-9.09 ± 0.09
F	$N_{\text{RFGC-UFG}} = 499$	45	124	145	100	40	45
	-10.61 ± 0.02	-11.08 ± 0.06	-10.82 ± 0.03	-10.6 ± 0.02	-10.5 ± 0.03	-10.39 ± 0.04	-10.09 ± 0.03
	$N_{\text{UFG}} = 226$	5	11	46	63	87	14
	-10.46 ± 0.02	-10.97 ± 0.18	-10.78 ± 0.08	-10.63 ± 0.04	-10.46 ± 0.03	-10.35 ± 0.03	-10.11 ± 0.07
	$N_{\text{RFGC-UFG}} = 423$	35	97	122	92	37	40
	-0.65 ± 0.03	-1.29 ± 0.08	-0.95 ± 0.05	-0.69 ± 0.04	-0.5 ± 0.04	-0.3 ± 0.05	0.06 ± 0.04
	$N_{\text{UFG}} = 201$	4	9	43	48	79	18
	-0.43 ± 0.03	-1.23 ± 0.41	-0.97 ± 0.13	-0.71 ± 0.08	-0.47 ± 0.06	-0.25 ± 0.03	0.02 ± 0.06
	$N_{\text{RFGC-UFG}} = 423$	35	97	122	92	37	40
	-0.39 ± 0.03	-0.07 ± 0.08	-0.21 ± 0.06	-0.34 ± 0.05	-0.53 ± 0.06	-0.62 ± 0.1	-0.74 ± 0.07
	$N_{\text{UFG}} = 201$	4	9	43	48	79	18
	-0.39 ± 0.04	0.06 ± 0.46	0.14 ± 0.22	-0.25 ± 0.07	-0.35 ± 0.08	-0.48 ± 0.05	-0.78 ± 0.09

Within the meaning of the P parameter, a typical ultra-flat galaxy is able to reproduce only 1/3 of its present stellar mass at the currently observed SFR. Consequently, the average SFR in thin disks was in the past approximately three times higher than in the present. If we assume that the M_*/L_K ratio is not equal to unity, but to $0.5 M_\odot/L_\odot$ [45], the average specific star formation rate in ultra-flat disks in the past would have been only by 0.13 dex, or 35% higher than that observed in the present. In this case, thin disks of galaxies would look like regular factories uniformly processing gas into stars. At that, the well-known observed 5–10-fold increase of the cosmic $SFR(z)$ in the epoch of $z \sim 1-3$ [52] would not have had any relation with the evolution of thin disks of galaxies. The value of the $\langle F \rangle$ parameter shows that a typical ultra-flat galaxy has reserves of gas, which allow to maintain the observed SFR for nearly 6 more billion years (if we do not consider internal extinction of the HI flux therein).

As is seen in Fig. 10, the P – F diagram has an elongation in the diagonal direction. This feature is due to the systematic increase in the specific SFR along the Hubble sequence from the early to late types. The FUV-flux measurement errors also lead to the scatter of galaxies in the diagonal direction.

Considering the sample of isolated galaxies from the 2MIG catalog [23], Melnyk et al. [21] obtained the mean parameters $\langle P \rangle = -0.62 \pm 0.02$ and

$\langle F \rangle = -0.14 \pm 0.02$. The value for 2MIG galaxies coincides within the errors with the mean -0.65 ± 0.03 for flat galaxies. However, the average parameter $\langle F \rangle = -0.39 \pm 0.03$ for flat and ultra-flat galaxies proves to be significantly smaller than the one for the isolated 2MIG disks. The reason for this difference is obviously due to internal extinction of the HI flux in strongly inclined galaxies. The RC3 catalog [34] and HyperLEDA give in addition to the m_{21} -magnitude the m_{21}^c -magnitudes too, corrected for internal extinction, according to [26]:

$$m_{21}^c = m_{21} - 2.5 \log(0.031 \sec i) + 2.5 \log[1 - \exp(0.31 \sec i)], \quad (14)$$

where i is the angle of inclination. At $i > 89^\circ$ the extinction is considered in RC3 to be the same and equal to 0^m82. We did not use the m_{21}^c -magnitude for the RFGC galaxies, assuming that this scheme is not enough applicable for the edge-on disks: firstly, the errors in determining the angle of inclination in them from the axial ratio a/b are sometimes considerable, and secondly, the amount of the extinction has to depend not only on the angle i , but also on the size (luminosity) of the galaxy. Nonetheless, the expected correction for galaxies with $a/b > 10$ based on the scheme [26] is on the average $\Delta m_{21} = 0^m5$, or $\Delta \log F_{\text{HI}} = 0.20$, the account of which eliminates the differences in $\langle F \rangle$ between the UFG and 2MIG galaxies. Wherein the estimate of

the characteristic time of depletion of gas in flat galaxies increases from 6 to 9 Gyrs. Furthermore, for six flat galaxies, the kinematics of which is investigated in [53], the mean underestimation of the hydrogen mass due to the extinction in the H I line amounts to $27 \pm 6\%$.

For the LOG catalog of isolated galaxies of the Local Supercluster [22] the authors have found median parameters $P = -0.05$ and $F = -0.03$. Comparing them with the values of $\langle P \rangle$ and $\langle F \rangle$ for the UFG sample, it should be taken into account that dwarf galaxies with large gas abundances and high SFR prevail in the near volume of the LOG catalog. As we have already noted, the error of determination of the FUV-flux in ultra-flat galaxies, residual uncertainty of the scheme of corrections for the internal extinction, as well as a yet vague systematics in estimating the stellar mass from the K -luminosity altogether lead to the scatter of UFG galaxies by

the P and F parameters of about 0.2–0.3 dex. This variation is somewhat smaller than the one observed (approximately by 0.4 dex). It is possible that the true distribution of the thin isolated disks on the diagnostic diagram P – F is very compact due to the uniform nature of the process of conversion of gas into stars [54]. To check this assumption, systematic programs of photometric and kinematic studies of ultra-flat galaxies, including the measurements of their $H\alpha$ fluxes and determining the rotation curves from the optical spectra are required.

ACKNOWLEDGMENTS

In this paper, we used the NED and HyperLEDA databases, as well as the data of GALEX, SDSS, 2MASS and WISE sky surveys. IDK thanks the Russian Science Foundation for the financial support within the grant no. 14-12-00965.

-
1. B. M. Tinsley, *Astrophys. J.* **151**, 547 (1968).
 2. R. B. Larson, B. M. Tinsley, and C. N. Caldwell, *Astrophys. J.* **237**, 692 (1980).
 3. R. C. Kennicutt, Jr., J. C. Lee, J. G. Funes, et al., *Astrophys. J. Suppl.* **178**, 247 (2008).
 4. R. C. Kennicutt, Jr., C.-N. Hao, D. Calzetti, et al., *Astrophys. J.* **703**, 1672 (2009).
 5. J. C. Lee, A. Gil de Paz, R. C. Kennicutt, Jr., et al., *Astrophys. J. Suppl.* **192**, 6 (2011).
 6. D. A. Thilker, L. Bianchi, G. Meurer, et al., *Astrophys. J. Suppl.* **173**, 538 (2007).
 7. V. Buat, T. T. Takeuchi, J. Iglesias-Páramo, et al., *Astrophys. J. Suppl.* **173**, 404 (2007).
 8. J. Brinchmann, S. Charlot, S. D. M. White, et al., *Monthly Notices Roy. Astronom. Soc.* **351**, 1151 (2004).
 9. K. G. Noeske, S. M. Faber, B. J. Weiner, et al., *Astrophys. J.* **660**, L47 (2007).
 10. L. E. Abramson, D. D. Kelson, A. Dressler, et al., *Astrophys. J.* **785**, L36 (2014).
 11. R. C. Kennicutt, Jr., *Annu. Rev. Astronom. Astrophys.* **36**, 189 (1998).
 12. Q. E. Goddard, R. C. Kennicutt, and E. V. Ryan-Weber, *Monthly Notices Roy. Astronom. Soc.* **405**, 2791 (2010).
 13. I. D. Karachentsev, S. S. Kaisin, and

- E. I. Kaisina, *Astrophysics* **58**, 453 (2015).
14. D. C. Martin, J. Fanson, D. Schiminovich, et al., *Astrophys. J.* **619**, L1 (2005).
 15. K. Abazajian, J. K. Adelman-McCarthy, M. A. Agüeros, et al., *Astronom. J.* **126**, 2081 (2003).
 16. M. F. Skrutskie, R. M. Cutri, R. Stiening, et al., *Astronom. J.* **131**, 1163 (2006).
 17. T. H. Jarrett, T. Chester, R. Cutri, et al., *Astronom. J.* **119**, 2498 (2000).
 18. T. H. Jarrett, F. Masci, C. W. Tsai, et al., *Astronom. J.* **144**, 68 (2012).
 19. I. D. Karachentsev and E. I. Kaisina, *Astronom. J.* **146**, 46 (2013).
 20. I. D. Karachentsev, V. E. Karachentseva, O. V. Melnyk, and H. M. Courtois, *Astrophysical Bulletin* **68**, 243 (2013).
 21. O. Melnyk, V. Karachentseva, and I. Karachentsev, *Monthly Notices Roy. Astronom. Soc.* **451**, 1482 (2015).
 22. I. D. Karachentsev, D. I. Makarov, V. E. Karachentseva, and O. V. Melnyk, *Astrophysical Bulletin* **66**, 1 (2011).
 23. V. E. Karachentseva, S. N. Mitronova, O. V. Melnyk, and I. D. Karachentsev, *Astrophysical Bulletin* **65**, 1 (2010).
 24. L. Morselli, A. Renzini, P. Popesso, and G. Erfanianfar, *Monthly Notices Roy. Astronom. Soc.* **462**, 2355 (2016).
 25. L. D. Matthews and W. van Driel, *Astron. Astrophys. Sup.* **143**, 421 (2000).
 26. J. Heidmann, N. Heidmann, and G. de Vaucouleurs, *Mem. Royal Astron. Soc.* **75**, 85 (1972).
 27. I. Karachentsev, *Astronom. J.* **97**, 1566 (1989).
 28. I. D. Karachentsev, V. E. Karachentseva, and S. L. Parnovskij, *Astronomische Nachrichten* **314**, 97 (1993).
 29. I. D. Karachentsev, V. E. Karachentseva, Y. N. Kudrya, et al., *Bull. Spec. Astrophys. Obs.* **47** (1999).
 30. V. E. Karachentseva, Y. N. Kudrya, I. D. Karachentsev, et al., *Astrophysical Bulletin* **71**, 1 (2016).
 31. I. D. Karachentsev, V. E. Karachentseva, and Y. N. Kudrya, *Astrophysical Bulletin* **71**, 129 (2016).
 32. D. Makarov, P. Prugniel, N. Terekhova, et al., *Astron. Astrophys.* **570**, A13 (2014).
 33. I. D. Karachentsev and D. A. Makarov, *Astronom. J.* **111**, 794 (1996).
 34. G. de Vaucouleurs, A. de Vaucouleurs, H. G. Corwin, Jr., et al., *Third Reference Catalogue of Bright Galaxies* (Springer-Verlag, New York, 1991).
 35. R. B. Tully, M. J. Pierce, J.-S. Huang, et al., *Astronom. J.* **115**, 2264 (1998).
 36. M. A. W. Verheijen and R. Sancisi, *Astron. Astrophys.* **370**, 765 (2001).
 37. B. M. Devour and E. F. Bell, *Monthly Notices Roy. Astronom. Soc.* **459**, 2054 (2016).
 38. A. H. Maller, A. A. Berlind, M. R. Blanton, and D. W. Hogg, *Astrophys. J.* **691**, 394 (2009).
 39. J. C. Lee, A. Gil de Paz, C. Tremonti, et al., *Astrophys. J.* **706**, 599 (2009).
 40. E. E. Salpeter, *Astrophys. J.* **121**, 161 (1955).
 41. P. Kroupa, *Monthly Notices Roy. Astronom. Soc.* **322**, 231 (2001).
 42. G. Chabrier, *Astrophys. J.* **586**, L133 (2003).
 43. E. F. Bell, D. H. McIntosh, N. Katz, and M. D. Weinberg, *Astrophys. J. Suppl.* **149**, 289 (2003).
 44. J. Binney and M. Merrifield, *Galactic Astronomy* (Princeton Univ. Press, Princeton, 1998).
 45. S. S. McGaugh and J. M. Schombert, *Astrophys.*

- J. **802**, 18 (2015).
46. T. H. Jarrett, T. Chester, R. Cutri, et al., *Astronom. J.***125**, 525 (2003).
 47. G. Meurer, arXiv:1608.05935 (2016).
 48. M. P. Haynes and R. Giovanelli, *Astronom. J.***89**, 758 (1984).
 49. T. H. Jarrett, F. Masci, C. W. Tsai, et al., *Astronom. J.***145**, 6 (2013).
 50. I. D. Karachentsev and S. S. Kaisin, *Astronom. J.***133**, 1883 (2007).
 51. M. Fukugita and P. J. E. Peebles, *Astrophys. J.* **616**, 643 (2004).
 52. P. Madau and M. Dickinson, *Annu. Rev. Astronom. Astrophys.***52**, 415 (2014).
 53. S. P. C. Peters, P. C. van der Kruit, R. J. Allen, and K. C. Freeman, *Monthly Notices Roy. Astronom. Soc.***464**, 32 (2017).
 54. A. Oemler, Jr., L. E. Abramson, M. D. Gladders, et al., ArXiv:1611.05932 (2016).

This figure "Melnik_fig6a.png" is available in "png" format from:

<http://arxiv.org/ps/1702.00266v1>